Admittance-Based Modeling of Transmission Lines by a Folded Line Equivalent

Bjørn Gustavsen, *Senior Member, IEEE*, and Adam Semlyen, *Life Fellow, IEEE*

***Abstract*—This paper describes a new transmission-line model for frequency-dependent modeling of untransposed overhead lines and underground cables. The nodal admittance matrix is decomposed into two blocks that, respectively, represent the open- and short-circuit conditions of a half-length line obtained by "folding" about the middle. By subjecting these matrices to rational fitting with inverse magnitude weighting, one obtains a model where the eigenvalues of the associated nodal admittance matrix are effectively fitted with high relative accuracy. This is shown to overcome the error magnification problem that occurs with direct fitting of the nodal admittance matrix. In addition, the modeling process (fitting and passivity enforcement) becomes faster. We show that this folded line equivalent (FLE) is particularly suitable as a companion form for phase-domain traveling-wave-type models, to be used when the time step is selected shorter than the line travel time. In this situation, the required model order is low and so the FLE gives highly efficient time-domain simulations.**

***Index Terms*—Electromagnetic transients, passivity enforcement, rational model, simulation, transmission line, vector fitting.**

I. Introduction

FREQUENCY-DEPENDENT transmission-line models are routinely applied in electromagnetic transients (EMT) programs for the representation of overhead lines and underground cables. The modeling techniques have undergone a profound development during the last 35 years due to the development of advanced computational techniques and faster computers.

The method of characteristics (MoC), also known as the traveling-wave method, is recognized as the preferred type of approach due to its efficiency and ability to handle wide frequency bands. Models within this class are either based on a constant transformation matrix with frequency-dependent modal propagation constants [1], [2], or a direct phase-domain modeling approach [3], [4]. In all methods, rational fitting and time delay extraction are central parts of the algorithm, leading to fast simulation by recursive convolution [1] or numerical integration.

Manuscript received February 08, 2008; revised April 21, 2008. Current version published December 24, 2008. This work was supported in part by the Norwegian Research Council (PETROMAKS Programme), in part by Compagnie Deutsch, in part by FMC Technologies, in part by Framo, in part by Norsk Hydro, in part by Siemens, in part by Statoil, in part by Total, and Vetco Gray. Paper no. TPWRD-00088-2008.

B. Gustavsen is with SINTEF Energy Research, Trondheim N-7465, Norway (e-mail: bjorn.gustavsen@sintef.no).

A. Semlyen is with the Department of Electrical and Computer Engineering, University of Toronto, Toronto, ON M5S 3G4, Canada (e-mail: adam.semlyen@utoronto.ca).

Color versions of one or more of the figures in this paper are available online at http://ieeexplore.ieee.org.

Digital Object Identifier 10.1109/TPWRD.2008.2002960

The application of an MoC-based transmission-line model requires that the time step used by the simulation engine (PSCAD/EMTP/ATP) be smaller than the line time delay. This leads to a dilemma in the modeling of a system that includes long and short lines as the short lines may require using a very small time step. Traditionally, this problem has been overcome by modeling the short lines by a cascade of PI-sections, but this modeling makes it difficult to include frequency-dependent effects [5]. Limitations in the handling of frequency dependency also exist with the alternative line model described in [6].

An alternative to the use of PI-sections is to model the line from its nodal admittance matrix $\mathbf{Y}_{\mathrm{nod}}$ in the frequency domain using rational fitting techniques. Unfortunately, the resulting model is often inaccurate with high-impedance terminations since $\mathbf{Y}_{\mathrm{nod}}$ is characterized by a large eigenvalue ratio at low frequencies. The accuracy problem can be overcome by application of the modal vector fitting (MVF) method [7], but the computation time can be substantial.

In this paper, we describe an alternative admittance-based formulation, the folded line equivalent (FLE), which decomposes $\mathbf{Y}_{\mathrm{nod}}$ into open-circuit and short-circuit contributions. This model allows retaining the relative accuracy of the eigenvalues of $\mathbf{Y}_{\mathrm{nod}}$ in the fitting process, thereby making the model applicable with arbitrary terminal conditions. The modeling is done in the phase domain without assumption of a constant transformation matrix, thereby being applicable to both overhead lines (transposed and untransposed) and underground cables. The rational modeling is based on the vector-fitting (VF) method [8] and so a computationally efficient approach is achieved. It is proposed that the EMT host program automatically replaces the MoC-based model with the FLE model when the time step length is chosen to be longer than the line travel time. That way, the required bandwidth of the admittance-based model (FLE) becomes limited so that a low order model is adequate. The paper describes every step in the modeling process: rational fitting, passivity assessment, passivity enforcement, and time-domain implementation. The advantages of the FLE and suggested replacement strategy are demonstrated by numerical examples.

II. Admittance-Based Transmission-Line Modeling

We start by reviewing one particular difficulty in the frequency-dependent modeling of transmission lines, namely the coexistence of large and small eigenvalues of the nodal admittance matrix at low frequencies (large eigenvalue ratio). Here, a given voltage application results in large currents if it represents a short circuit while it produces small currents if it corresponds to an open-circuit voltage (capacitive charging currents). The situation worsens when the line length is reduced as the short-circuit currents increase while the charging currents decrease.

This is not a problem with topologically correct models, such as a cascade of PI-sections, as the circuit branches are selected so as to correspond to the physical current flow. This is also not much of a problem in models based on diagonalization [18], since the individual modeling of the modes leads to accurate representation of the short-circuit currents and charging currents. On the other hand, the assumption of a constant eigenvector matrix reduces the model accuracy.

In phase-domain-type modeling, however, one performs rational modeling on elements that contains contributions from large and small eigenvalues. This requires the ability to fit the matrix elements to a very high accuracy in order to capture the information of the small eigenvalues.

However, for the direct phase-domain modeling from the nodal admittance matrix $\mathbf{Y}_{\rm nod}$, the large eigenvalue spread poses a difficulty in the modeling. $\mathbf{Y}_{\rm nod}$ defines the relation between port voltages and currents at the line ends (1), where all matrix/column quantities are frequency-dependent. The dimension of $\mathbf{Y}_{\rm nod}$ is $2n \times 2n$ where n is the number of (bundled) conductors

$$\mathbf{i}(\omega) = \mathbf{Y}_{\rm nod}(\omega)\mathbf{v}(\omega). \tag{1}$$

Applying currents to the ports rather than voltages, results in the response (voltage) becoming defined by the nodal impedance matrix $\mathbf{Z}_{\rm nod}$. Diagonalizing $\mathbf{Y}_{\rm nod}$ and carrying out the matrix inversion (2) shows that the small eigenvalues of $\mathbf{Y}_{\rm nod}$ become the large eigenvalues of $\mathbf{Z}_{\rm nod}$. Thus, the modeling from $\mathbf{Y}_{\rm nod}$ also requires accurately capturing the small eigenvalues. Otherwise, catastrophic error magnifications can take place

$$\mathbf{Z}_{\rm nod} = \mathbf{Y}_{\rm nod}^{-1} = \left(\mathbf{T}_Y \mathbf{\Lambda}_Y \mathbf{T}_Y^{-1}\right)^{-1} = \mathbf{T}_Y \mathbf{\Lambda}_Y^{-1} \mathbf{T}_Y^{-1}. \tag{2}$$

In [7], this problem was overcome by introducing the modal vector fitting, which seeks to minimize the error in the modal contributions, each weighted with the inverse eigenvalue magnitude in the associated least-squares (LS) problem (3)

$$\frac{1}{|\lambda_i|}(\mathbf{Y}_{\rm rat}\,\mathbf{t}_i - \lambda_i\,\mathbf{t}_i) \cong 0, \quad i = 1, \ldots, n. \tag{3}$$

The success of the MVF for transmission-lines modeling was demonstrated in [7]. Unfortunately, the computation time is quite substantial due to a less-sparse system matrix than in the classical VF formulation.

III. Folded Line Equivalent

A. Folding

Since the two line ends 1 and 2 are interchangeable, the admittance matrix obtains the block structure (4). In addition, $\mathbf{Y}_s$ and $\mathbf{Y}_m$ in (4) must be symmetrical. While this property of longitudinal symmetry is elementary and fairly trivial, it has not normally been paid attention to or recognized as a means for improving the efficiency of modeling. It is essential to the developments in this paper

$$\begin{bmatrix}\mathbf{i}_1\\ \mathbf{i}_2\end{bmatrix} = \begin{bmatrix}\mathbf{Y}_s & \mathbf{Y}_m\\ \mathbf{Y}_m & \mathbf{Y}_s\end{bmatrix}\begin{bmatrix}\mathbf{v}_1\\ \mathbf{v}_2\end{bmatrix}. \tag{4}$$

The structure in (4) can be utilized in the modeling by introducing the similarity transformation (5), (6), [17]

$$\begin{bmatrix}\mathbf{v}_1\\ \mathbf{v}_2\end{bmatrix} = \mathbf{K}\begin{bmatrix}\mathbf{v}_{\rm oc}\\ \mathbf{v}_{\rm sc}\end{bmatrix}, \begin{bmatrix}\mathbf{i}_1\\ \mathbf{i}_2\end{bmatrix} = \mathbf{K}\begin{bmatrix}\mathbf{i}_{\rm oc}\\ \mathbf{i}_{\rm sc}\end{bmatrix} \tag{5}$$

$$\mathbf{K} = \begin{bmatrix}\mathbf{I} & \mathbf{I}\\ \mathbf{I} & -\mathbf{I}\end{bmatrix}. \tag{6}$$

Combining (5) and (6) with (4) leads to the alternative admittance formulation (7), (8)

$$\begin{bmatrix}\mathbf{i}_{\rm oc}\\ \mathbf{i}_{\rm sc}\end{bmatrix} = \tilde{\mathbf{Y}}_{\rm nod}\begin{bmatrix}\mathbf{v}_{\rm oc}\\ \mathbf{v}_{\rm sc}\end{bmatrix} \tag{7}$$

$$\begin{aligned}\tilde{\mathbf{Y}}_{\rm nod} &= \begin{bmatrix}\mathbf{Y}_s + \mathbf{Y}_m & \mathbf{0}\\ \mathbf{0} & \mathbf{Y}_s - \mathbf{Y}_m\end{bmatrix}\\ &= \begin{bmatrix}\mathbf{Y}_{\rm oc} & \mathbf{0}\\ \mathbf{0} & \mathbf{Y}_{\rm sc}\end{bmatrix}.\end{aligned} \tag{8}$$

$\mathbf{Y}_{\rm oc}$ represents the (open circuit) current response when applying the same voltage to both line ends, while $\mathbf{Y}_{\rm sc}$ represents the (short circuit) current response when the applied voltage at the two line ends are equal but of opposite polarity. The longitudinal distribution of voltage and current along the line appears as even functions $(\mathbf{Y}_{\rm oc})$ and odd functions $(\mathbf{Y}_{\rm sc})$ with respect to the line center point, as at the fold of a sheet of paper. We therefore refer to this formulation (7),(8) as the folded line equivalent (FLE). We may even call folding the particular similarity transformation used above based on the longitudinal symmetry of the line.

The FLE realization can be transformed back into the original phase coordinates via the transformation (9)

$$\begin{aligned}\mathbf{Y}_{\rm nod} &= \mathbf{K}\begin{bmatrix}\mathbf{Y}_{\rm oc} & \mathbf{0}\\ \mathbf{0} & \mathbf{Y}_{\rm sc}\end{bmatrix}\mathbf{K}^{-1}\\ &= \frac{1}{2}\begin{bmatrix}\mathbf{Y}_{\rm oc} + \mathbf{Y}_{\rm sc} & \mathbf{Y}_{\rm oc} - \mathbf{Y}_{\rm sc}\\ \mathbf{Y}_{\rm oc} - \mathbf{Y}_{\rm sc} & \mathbf{Y}_{\rm oc} + \mathbf{Y}_{\rm sc}\end{bmatrix}.\end{aligned} \tag{9}$$

B. Accuracy Considerations

As was noted in Section II, fitting an admittance matrix having a large eigenvalue ratio can lead to catastrophic error magnifications in applications with high impedance terminal conditions. Equation (10) shows that with FLE, the matrix inversion (2) leads to the inverse of $\mathbf{Y}_{\rm oc}$ and $\mathbf{Y}_{\rm sc}$. These matrices have each a small eigenvalue ratio since they, respectively, correspond to open-circuit and short-circuit conditions. It follows that by subjecting $\mathbf{Y}_{\rm oc}$ and $\mathbf{Y}_{\rm sc}$, rather than $\mathbf{Y}_{\rm nod}$, to rational fitting, the error magnification problem can be avoided

$$\begin{aligned}\mathbf{Z}_{\rm nod} = \mathbf{Y}_{\rm nod}^{-1} &= \left(\mathbf{K}\begin{bmatrix}\mathbf{Y}_{\rm oc} & \mathbf{0}\\ \mathbf{0} & \mathbf{Y}_{\rm sc}\end{bmatrix}\mathbf{K}^{-1}\right)^{-1}\\ &= \mathbf{K}\begin{bmatrix}\mathbf{Y}_{\rm oc}^{-1} & \mathbf{0}\\ \mathbf{0} & \mathbf{Y}_{\rm sc}^{-1}\end{bmatrix}\mathbf{K}^{-1}.\end{aligned} \tag{10}$$

C. FLE Properties

The following remarks can be made about the transformed description.

1) $\tilde{\mathbf{Y}}_{\rm nod}$ is block diagonal with each block being half the size of $\mathbf{Y}_{\rm nod}$.
2) $\mathbf{Y}_{\rm oc}$ and $\mathbf{Y}_{\rm sc}$ are symmetric matrices.
3) The combined set of eigenvalues of $\mathbf{Y}_{\rm oc}$ and $\mathbf{Y}_{\rm sc}$ is equal to the eigenvalues of $\mathbf{Y}_{\rm nod}$.
4) If $\mathbf{x}_{\rm oc}, \mathbf{x}_{\rm sc}$ are eigenvectors of $\mathbf{Y}_{\rm oc}$ and $\mathbf{Y}_{\rm sc}$, respectively, then the corresponding eigenvectors of $\mathbf{Y}_{\rm nod}$ are

$$[\mathbf{x}_{\rm oc}^T \quad \mathbf{x}_{\rm oc}^T]^T \quad \text{and} \quad [\mathbf{x}_{\rm sc}^T \quad -\mathbf{x}_{\rm sc}^T]^T.$$

5) The eigenvalue ratio (ratio between largest and smallest eigenvalue) is moderate (at low frequencies) for $\mathbf{Y}_{\rm oc}$ and $\mathbf{Y}_{\rm sc}$ while it is large for $\mathbf{Y}_{\rm nod}$.

IV. Rational Fitting And Passivity Enforcement

A. Symmetric Matrix Fitting With Relative Error Control

The blocks $\mathbf{Y}_{\rm oc}$ and $\mathbf{Y}_{\rm sc}$ are fitted independently, each with a private pole set. The symmetry of each block is retained by stacking the elements of the upper (or lower) triangle into a common vector that is fitted by VF (with relaxation of the non-triviality constraint [9]). In the fitting process, we require that the representations be asymptotically correct, leading to models (11) and (12), where $\mathbf{Y}_c(\infty)$ is the characteristic admittance of the line at the infinite frequency. For the VF least-squares (LS) problems, we apply inverse magnitude weighting with the matrix norms (13), thereby fitting with relative error control

$$\mathbf{Y}_{\rm oc}(\omega) \cong \sum_{m=1}^{N} \frac{\mathbf{R}_{{\rm oc},m}}{j\omega - a_{{\rm oc},m}} + \mathbf{Y}_c(\infty) \tag{11}$$

$$\mathbf{Y}_{\rm sc}(\omega) \cong \sum_{m=1}^{N} \frac{\mathbf{R}_{{\rm sc},m}}{j\omega - a_{{\rm sc},m}} + \mathbf{Y}_c(\infty) \tag{12}$$

$$\begin{aligned} \text{weight}_{\rm oc}(\omega) &= \frac{1}{||\mathbf{Y}_{\rm oc}(\omega)||_2}, \\ \text{weight}_{\rm sc}(\omega) &= \frac{1}{||\mathbf{Y}_{\rm sc}(\omega)||_2}. \end{aligned} \tag{13}$$

In order to enforce the asymptotic high-frequency property of (11), we subject $\mathbf{Y}_{\rm oc} - \mathbf{Y}_c(\infty)$ and $\mathbf{Y}_{\rm sc} - \mathbf{Y}_c(\infty)$ to fitting with the zero constant term, with (13) as LS weighting.

B. Fast Passivity Assessment

The extracted model must be passive in order to ensure a stable simulation. The model is passive if its conductance matrix $\mathbf{G}(\omega)$ is positive definite for all frequencies [10], i.e.,

$$\text{eig}(\mathbf{G}_{\rm nod}(\omega)) = \text{eig}(\Re\{\mathbf{Y}_{\rm nod}(\omega)\}) > 0. \tag{14}$$

As noted, the eigenvalues of $\tilde{\mathbf{Y}}_{\rm nod}$ (8) are equal to the combined set of eigenvalues from $\mathbf{Y}_{\rm oc}$ and $\mathbf{Y}_{\rm sc}$. Therefore, the passivity assessment can be made for the models of $\mathbf{Y}_{\rm oc}$ and $\mathbf{Y}_{\rm sc}$ independently. The passivity assessment is done via the singularity test matrix (STM) [11], $\mathbf{S}$ in (15). Here, the pole-residue models have first been expanded into real-only state-space models ($\mathbf{A}$, $\mathbf{B}$, $\mathbf{C}$, $\mathbf{D}$), see [11, App.]. The singularity test matrix $\mathbf{S}$ gives, via the subset of its positive-real eigenvalues ω^2, the frequencies ω where $\mathbf{G}_{\rm nod}$ becomes singular and these are the boundaries of passivity violations

$$\mathbf{S} = \mathbf{A}(\mathbf{B}\mathbf{D}^{-1}\mathbf{C} - \mathbf{A}). \tag{15}$$

The application of $\mathbf{S}$ to $\mathbf{Y}_{\rm oc}$ and $\mathbf{Y}_{\rm sc}$ instead of $\mathbf{Y}_{\rm nod}$ gives a computational speed-up by a factor of four, since the time needed for eigenvalues computations increases cubically with the matrix size. Note that $\mathbf{S}$ is only half the size of the Hamiltonian matrix $\mathbf{M}$ that has traditionally been used for passivity assessment [12], [13]. Usage of $\mathbf{S}$ rather than $\mathbf{M}$ leads additionally to eight times faster computations. Combined with the usage of $\mathbf{Y}_{\rm oc}$ and $\mathbf{Y}_{\rm sc}$, a total speedup by a factor of $8 \times 4 = 32$ is obtained.

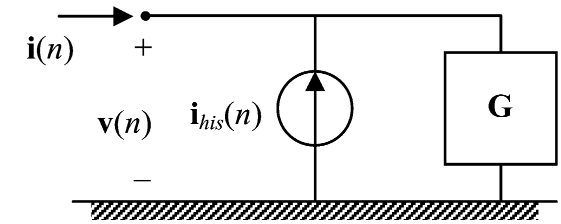

Fig. 1. Norton equivalent representation of $\mathbf{Y}_{\rm oc}$ and $\mathbf{Y}_{\rm sc}$.

C. Passivity Enforcement by Fast Modal Perturbation

Any remaining passivity violations are removed by subjecting the rational model to perturbation. For that purpose, we apply the fast modal perturbation (FMP) approach [14], which is based on the perturbation concept introduced in [15]. FMP enforces passivity by perturbing the eigenvalues of each residue matrix while minimizing the error of the admittance eigenvalues in the relative sense. The approach includes a robust iteration scheme which adds new samples to the constraint part of the quadratic-programming (QP) formulation to prevent new passivity violations from appearing. Since the computation time of the basic steps in QP increases cubically with problem size (number of free variables), enforcing passivity for (the half-size) $\mathbf{Y}_{\rm oc}$ and $\mathbf{Y}_{\rm sc}$ instead of $\mathbf{Y}_{\rm nod}$ can be expected to give a speedup by a factor of four.

V. Numerical Integration for the Time Step Loop

Using trapezoidal integration (or recursive convolution [1]), a Norton equivalent (Fig. 1) is established for each of the two pole-residue models ($\mathbf{Y}_{\rm oc}$ and $\mathbf{Y}_{\rm sc}$). The Norton equivalents are combined into a single equivalent by the following transformations:

$$\mathbf{G} = \mathbf{K}\begin{bmatrix} \mathbf{G}_{\rm oc} & \mathbf{0} \\ \mathbf{0} & \mathbf{G}_{\rm sc} \end{bmatrix}\mathbf{K}^{-1} \tag{16}$$

$$\begin{bmatrix} \mathbf{i}_{1,\rm his} \\ \mathbf{i}_{2,\rm his} \end{bmatrix} = \mathbf{K}\begin{bmatrix} \mathbf{i}_{\rm oc,his} \\ \mathbf{i}_{\rm sc,his} \end{bmatrix}. \tag{17}$$

In each time step, the node voltages are transformed into $\mathbf{v}_{\rm oc}$ and $\mathbf{v}_{\rm sc}$ by the transformation (5) (left equation), which are used as excitations in a columnwise realization of the convolution. Further details on the implementation of the convolution for pole-residue models can be found in [16].

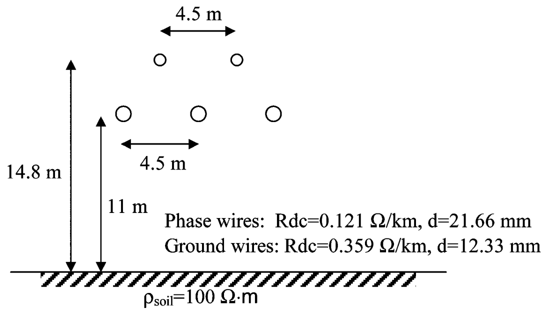

Fig. 2. Three-phase overhead line.

VI. Example: Three-Phase Overhead Line

A. Line Configuration

As an example, we consider the modeling of a 132-kV overhead line of 300-m length, see Fig. 2. This gives a lossless time delay of about 1 μs. The line is modeled via its series impedance and shunt capacitance while taking into account the skin effect in conductors and earth.

B. Modeling Alternatives and Simulation Approach

The overhead line is to be modeled by the following alternatives:

1) FLE;
2) universal line model (ULM) [4];
3) direct fitting of $\mathbf{Y}_{\rm nod}$.

All frequency-domain calculations (line constants and rational modeling) are done in Matlab in order to make the calculations directly comparable. A small conductance is added to the diagonal elements to achieve a controlled behavior at dc conditions.

With FLE, all time-domain simulations are done using a small EMTP-like program based on trapezoidal integration. The same program is used when modeling the line by direct fitting of $\mathbf{Y}_{\rm nod}$.

With ULM (MoC-based model), the matrices of propagation $\mathbf{H}$ and characteristic admittance $\mathbf{Y}_c$ are fitted in the frequency band 1 Hz-10 MHz, within the Matlab environment. The rational model is read into the PSCAD environment to permit a regular PSCAD simulation.

With the PI-equivalent, the matrix of series impedance is evaluated at the dominant frequency component in the simulation, and the capacitance matrix is distributed evenly between the two line ends. This defines a coupled, single-stage equivalent. The simulation is done in the Matlab environment.

C. FLE: Rational Fitting and Passivity Enforcement

Since the (lossless) travel time of the line is $\tau = 1$ μs, the FLE should replace the MoC-based model whenever the simulation time step is chosen to be larger than 1 μs. We thus require the FLE to be accurate up to 1 MHz.

Fig. 3 shows the fitting result for $\mathbf{Y}_{\rm oc}$ and $\mathbf{Y}_{\rm sc}$ after rational fitting (1 Hz-1 MHz) and passivity enforcement. The fitting used 18 pole-residue terms. The deviation traces are seen to be almost parallel to the respective element traces, indicating a relative error criterion. Fig. 4 shows the result for $\mathbf{Y}_{\rm nod}$ after expanding the model by (9).

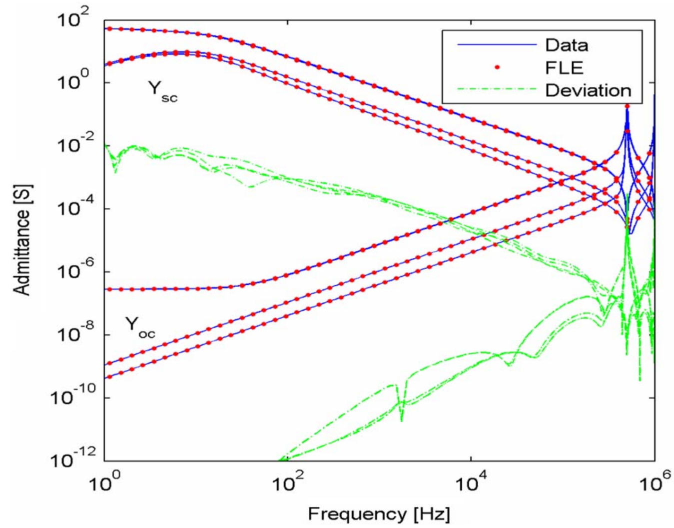

Fig. 3. Rational modeling of $\mathbf{Y}_{\rm oc}$ and $\mathbf{Y}_{\rm sc}$. Fourteenth-order fitting.

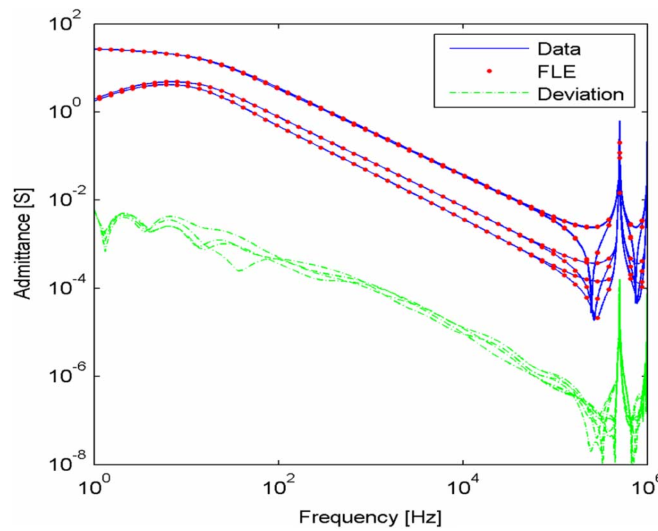

Fig. 4. Elements of $\mathbf{Y}_{\rm nod}$.

Fig. 5 shows a result from the passivity enforcement step. A passivity violation was detected via the singularity test matrix (15), which shows a negative eigenvalue in $\mathbf{G}_{\rm nod}$. The passivity violation was corrected by FMP in a single iteration.

D. Accuracy Assessment

Fig. 6 compares the condition numbers of $\mathbf{Y}_{\rm nod}$, $\mathbf{Y}_{\rm oc}$, and $\mathbf{Y}_{\rm sc}$. The condition number κ defines the ratio between the largest and smallest singular value. (This is an alternative precise measure of the eigenvalue ratio since for a square matrix $\mathbf{A}$, the singular values are equal to the square root of the eigenvalues of $\mathbf{A}^H\mathbf{A}$, where H denotes transpose and conjugate). It is seen that $\mathbf{Y}_{\rm nod}$ has a large κ at low frequencies while that of $\mathbf{Y}_{\rm oc}$ and $\mathbf{Y}_{\rm sc}$ are small. The small κ means a small eigenvalue ratio for these matrices, implying that a rational model based on $\mathbf{Y}_{\rm oc}$ and $\mathbf{Y}_{\rm sc}$ will have all of its eigenvalues accurate in the relative sense. This assertion is verified in Fig. 7, where the

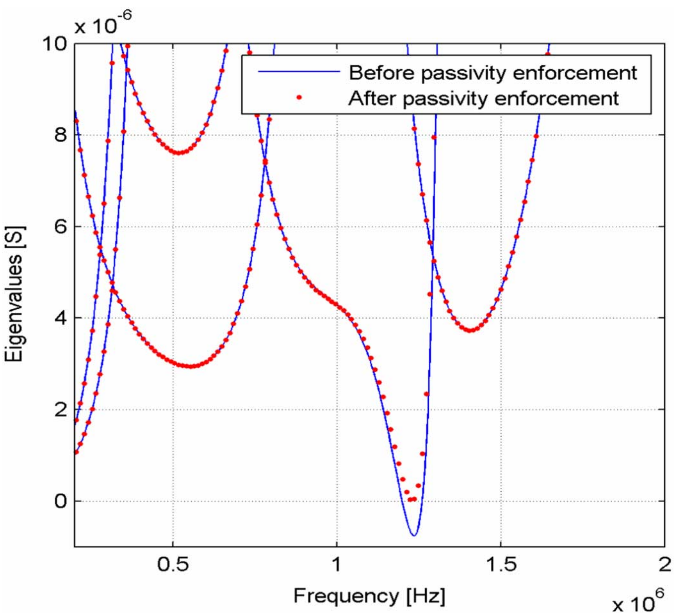

Fig. 5. Eigenvalues of $\mathbf{G}_{\mathrm{nod}}$ (rational model).

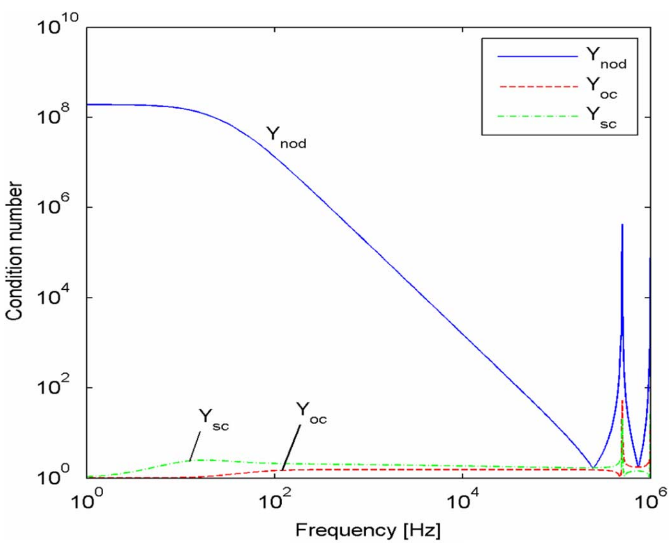

Fig. 6. Condition numbers: $\mathbf{Y}_{\mathrm{nod}}$, $\mathbf{Y}_{\mathrm{oc}}$, and $\mathbf{Y}_{\mathrm{sc}}$.

FLE-based model has been expanded by (9). As a consequence, $\mathbf{Y}_{\mathrm{nod}}$ can be inverted with only small error magnifications (see Fig. 8), thus allowing the model to be applied with arbitrary terminal conditions.

E. Simulation: FLE versus ULM

Fig. 9 shows a case where the transmission line is energized from a three-phase voltage source behind a short-circuit reactance. A single-phase ground fault occurs 0.5 ms after energization, near voltage maximum.

Fig. 10 shows the simulated voltage response at the far line end, obtained using either ULM (PSCAD environment), or FLE (Matlab environment). The response is essentially a 9.8-kHz resonance between the line capacitance and the feeding reactance, superimposed on the 50-Hz feeding voltage. It can be seen that the result by the two approaches is in close agreement. The

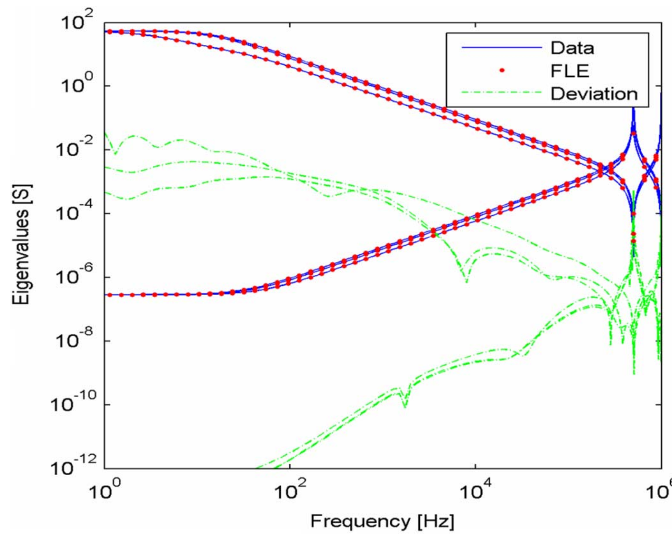

Fig. 7. Eigenvalues of $\mathbf{Y}_{\mathrm{nod}}$.

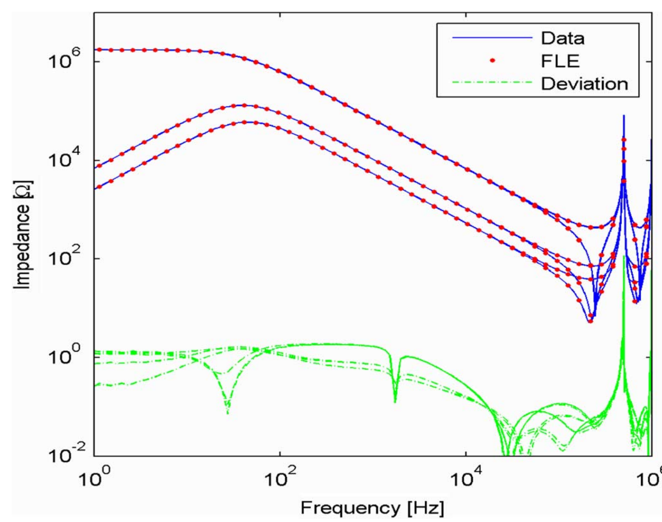

Fig. 8. Elements of $\mathbf{Z}_{\mathrm{nod}} = \mathbf{Y}_{\mathrm{nod}}^{-1}$.

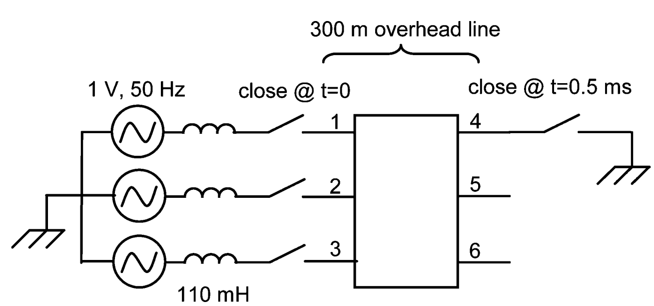

Fig. 9. Line energization and ground fault initiation.

ULM modeling used 12 poles for $\mathbf{Y}_c$ and 14 poles for $\mathbf{H}$ with a single delay group. The simulation time step is 1 μs with FLE and 0.1 μs with ULM. For comparison, the lossless delay of the line is 1 μs.

Fig. 11 shows the same result when increasing the simulation time step to 4 μs in FLE and ULM, thus being four times bigger than the line travel time (1 μs). It is seen that FLE still produces the correct result whereas the result by ULM is highly

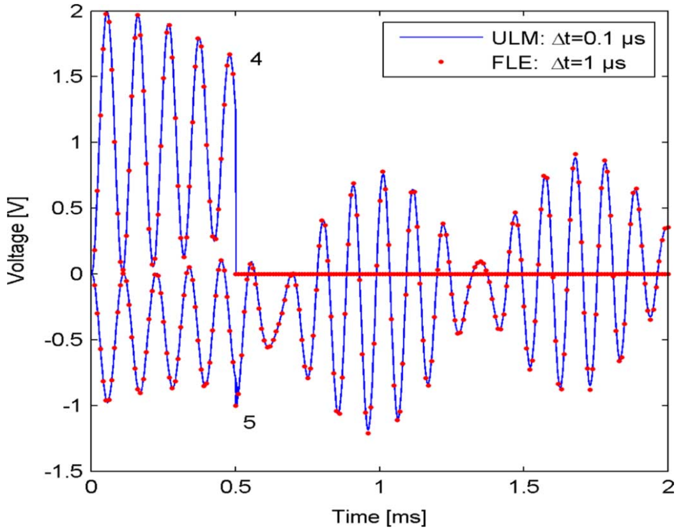

Fig. 10. Far-end voltage response.

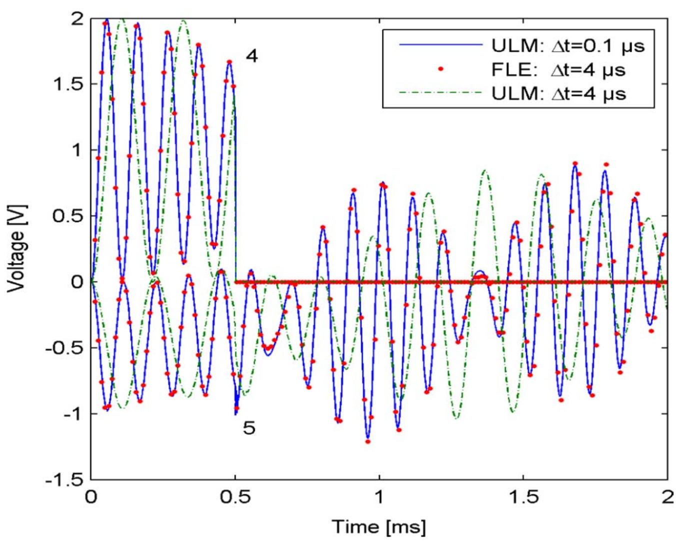

Fig. 11. Far-end voltage response. Increasing the time step beyond τ.

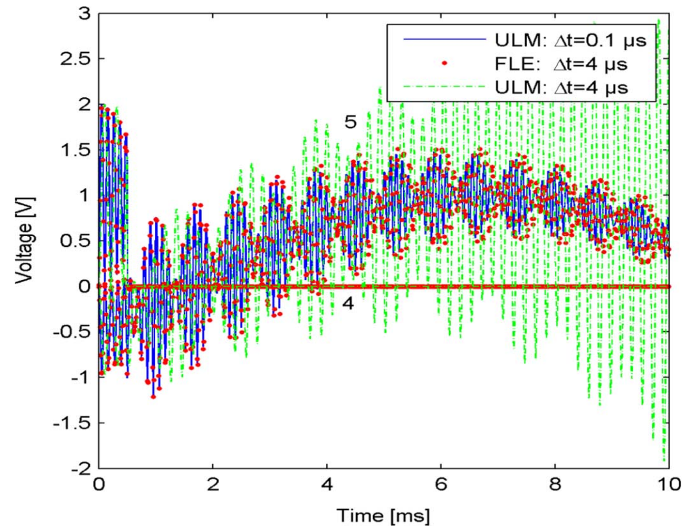

Fig. 12. Far-end voltage response. Extended view.

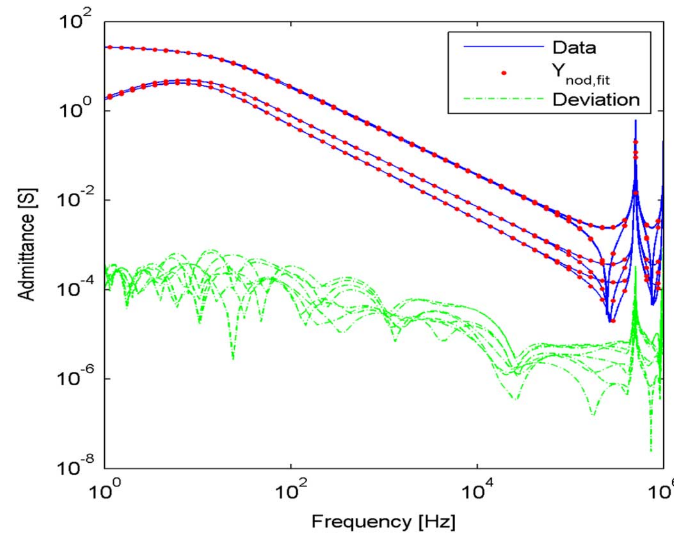

Fig. 13. Direct fitting of $\mathbf{Y}_{\mathrm{nod}}$ (26 pole-residue terms).

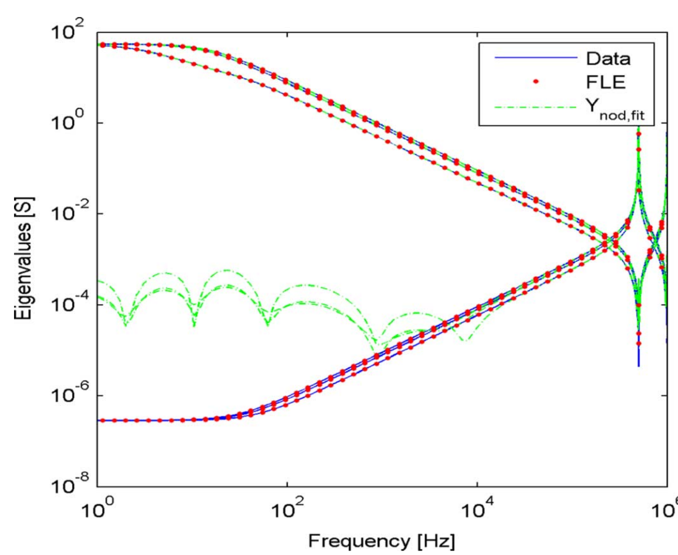

Fig. 14. Eigenvalues of $\mathbf{Y}_{\mathrm{nod}}$.

inaccurate. The extended plot in Fig. 12 shows that the result by ULM is unstable. (The instability problem also persisted when calculating the model parameters using PSCAD's built-in line constants and fitting routines.)

F. Limitations of Direct Fitting Approach

An alternative to the FLE approach is to fit $\mathbf{Y}_{\mathrm{nod}}$ directly. Fig. 13 shows the result after rational fitting and passivity enforcement using 26 pole-residue terms. The accuracy is not much different from that of the FLE model (Fig. 4), but a look at the eigenvalues of $\mathbf{Y}_{\mathrm{nod}}$ (Fig. 14) shows that the small eigenvalues have been corrupted. As a consequence, the model is incapable of simulating the far-end transient voltage (Fig. 15) since the response is essentially an oscillation between the line capacitance and the feeding inductance. This oscillation mode involves the small eigenvalues of $\mathbf{Y}_{\mathrm{nod}}$; in Fig. 15, they are seen to be inaccurately represented at the dominant frequency (9.8 kHz).

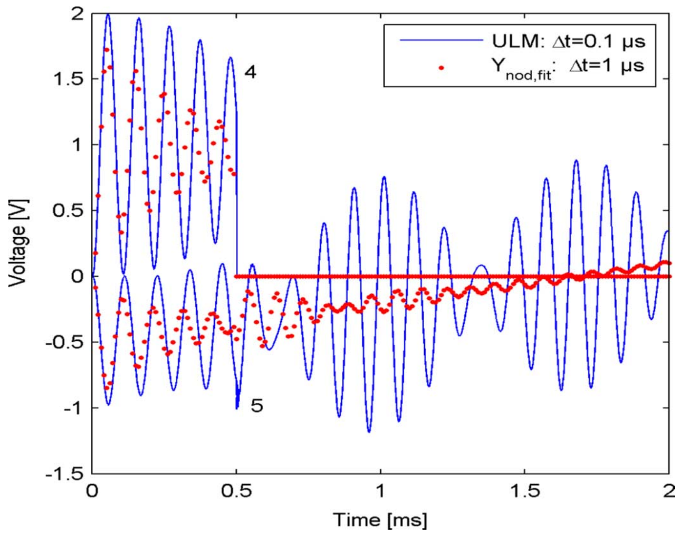

Fig. 15. Far-end voltage response.

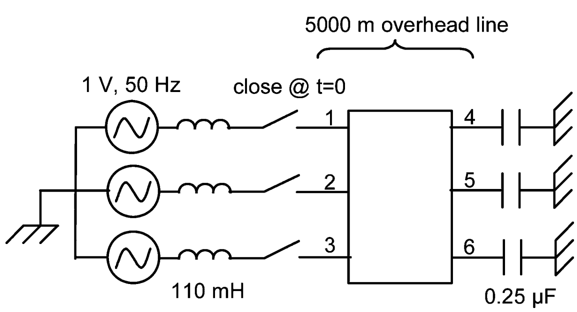

Fig. 16. Energizing 5-km overhead line connected to 1-km cable.

G. Limitations of PI-Sections Approach

An alternative to the FLE approach is to represent the line/cable with a cascade of (coupled) PI-sections. This offers a straightforward solution which does not require rational fitting or passivity enforcement. One disadvantage of PI-sections is that they are accurate only at a single frequency. This makes it difficult to automate the replacement of a traveling-wave model since the specification of a representative frequency is not straightforward. The frequency must be either a user-defined frequency or some characteristic frequency (e.g., the system operating frequency or the line quarter-wave frequency).

We demonstrate the limitation of the PI-sections approach with the circuit in Fig. 16. The transmission-line length is increased to 5 km and it is connected to 0.25-μF capacitors at the far end, which approximately represents a 1-km-long cable.

Fig. 17 shows the far-end voltage response as simulated using the ULM-model of PSCAD with a 1-μs time step. The dominant frequency component is 862 Hz, superimposed on the 50-Hz voltage.

Fig. 18 shows the deviation from the response by ULM when modeling the line using either FLE or a cascade of three PI-sections. The PI-sections are calculated at either 50 Hz, 862 Hz, or 15000 Hz (quarter-wave resonance frequency of the line). It is seen that the FLE gives a very small deviation whereas the PI-section approach gives a much higher deviation, unless its parameters are calculated at the dominant frequency component

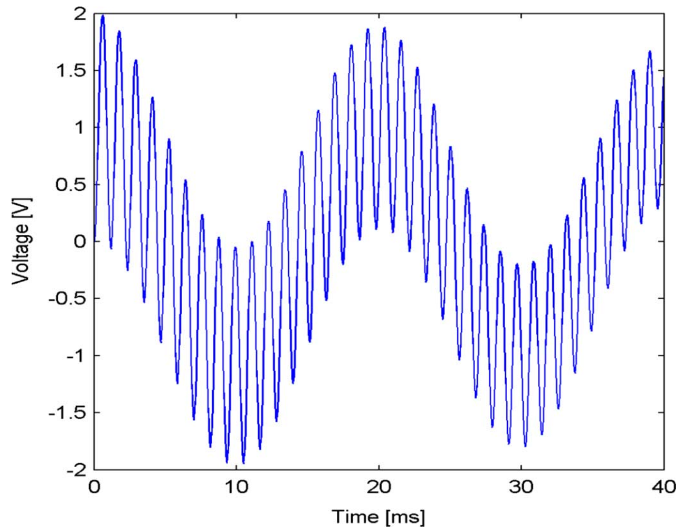

Fig. 17. Far-end voltage response at node 4 (ULM). $\Delta t = 1\ \mu$s.

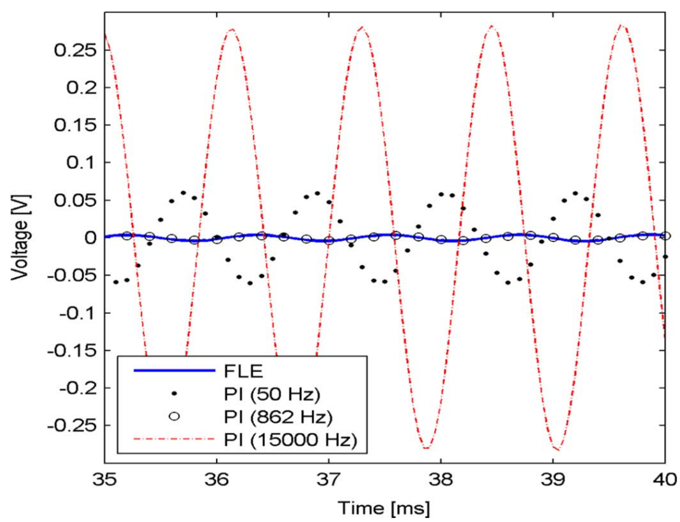

Fig. 18. Deviation from the ULM response $\Delta t = 1\ \mu$s.

(862 Hz). The nature of the error is incorrect attenuation of the transient, not a phase shift.

The slow nature of the transient allows increasing the time step considerably. Fig. 19 compares the response by ULM and a 1-μs time step with that by FLE and a 50-μs time step. (In the simulation with ULM, the voltage source was ramped up linearly in 50 μs). The peak values are seen to be well represented although a small phase shift develops with time. This phase shift is due to the numerical integration since each period of the 862-Hz component is with a 50-μs time step represented by only 23 time steps. It is noted that the line travel time of 16.7 μs is the maximum time step allowable with ULM.

Table I compares the peak value of the simulated voltage near $t = 30$ ms, depending on the line model. It is seen that the accuracy of FLE remains excellent whereas usage of the PI-equivalent calculated at 15 kHz gives much too strong attenuation.

VII. Timing Results

Table II lists the CPU times needed for some of the critical computational steps in the modeling of the overhead line

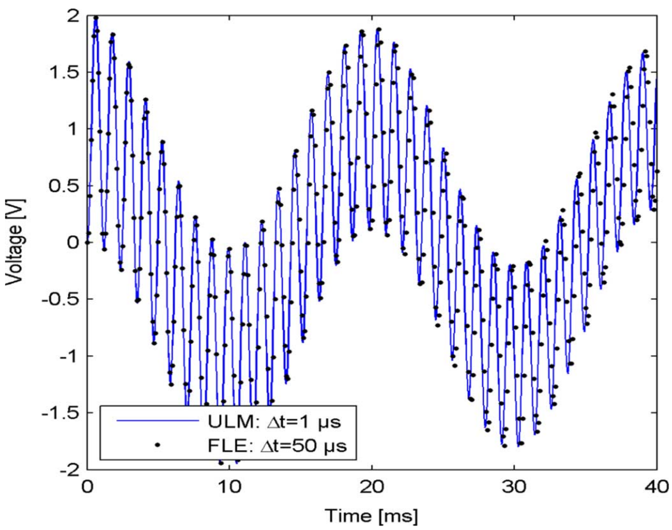

Fig. 19. FLE model with a 50-μs time step.

TABLE I
VOLTAGE PEAK VALUE

Model	Voltage [V]
ULM (Δt=1 μs)	–1.80
FLE (Δt=50 μs)	–1.79
PI (Δt=50 μs, *f*=50 Hz)	–1.83
PI (Δt=50 μs, *f*=862 Hz)	–1.79
PI (Δt=50 μs, *f*=15000 Hz)	–1.54

TABLE II
TIME CONSUMPTION (in seconds)

Task	Approach	
	FLE	Direct Fitting
Rational fitting (VF)	6.4	24.1
Passivity assessment (STM)	0.01	0.75
Passivity enforcement (quadprog)	1.9	10.0
Time domain simulation (10,000 time steps)	1.4	1.2

of 300-m length. There is, in addition, computational overhead, mainly in the passivity assessment step.

The first row gives the computation time spent by the VF-routine with 401 frequency samples. The fitting process used ten VF iterations on the matrix trace, followed by ten iterations on the full matrix. A QR-based solver was used with sparse computations. The direct fitting of $\mathbf{Y}_{\rm nod}$ is seen to take about four times longer to execute than the fitting of FLE. The comparison is made difficult by the fact that the model order was different—26 and 18, respectively, for the direct approach and FLE.

The second row shows the time needed for the eigenvalue computation in the passivity assessment step (15). The computation time for FLE is completely negligible (0.01 s) and it is also very small by the direct fitting approach. The longer computation time by the latter approach is partly caused by the need for several iterations to remove the passivity violations.

The third row states the time spent in the QP routine (quadprog.m) used by the FMP for solving the passivity enforcement step. With the direct fitting approach, five times longer time is spent by "quadprog." Again, the comparison is made with difficulty as the FMP needed many more iterations when applied to the result by the direct approach, and because the number of internal iterations in "quadprog" is case dependent.

The fourth row compares the computation time for simulating the circuit in Fig. 9 with 10 000 time steps. It is seen that the time consumption is in both cases is slightly above 1 s.

We conclude based on the above that the FLE leads, as expected, to significantly faster overall computation compared to direct fitting methods due to reduced matrix dimensions and simpler modeling but concrete quantitative predictions of timing cannot be realistic due to the complexity of the procedures involved.

VIII. DISCUSSION

This paper has focused on the situation where the simulation time step is chosen larger than the travel time of the line. This situation occurs frequently in practice as a circuit often has long and short lines. With the current practice, the user of an EMT program has to manually replace the MoC-based model with a cascaded PI-circuit whenever the time step becomes longer than the line travel time. If the substitution is not done, some EMT programs will terminate with an error message while others will still use the MoC-based model. As was shown in Section VI-E, the continued usage of an MoC-based model may result in an incorrect simulation or even an unstable result. On the other hand, it was shown in Section VI-G that usage of PI sections can lead to inaccurate results. The FLE model overcomes this problem since it takes all frequency-dependent effects into account, and it is not prone to error magnifications (unlike a model obtained by directly fitting $\mathbf{Y}_{\rm nod}$). Unfortunately, FLE is computationally inefficient for wideband representations since then the model order becomes very high.

A practical solution to this dilemma is to let the EMT program automatically switch between the MoC-based model and the FLE model, depending on the chosen time step versus the line delay. With this strategy, the frequency responses to be fitted in FLE will only contain a few resonances and so a low-order model is always obtained. In the calculated example (300-m line), the FLE used only 18 pole-residue terms for the fitting of $\mathbf{Y}_{\rm oc}$ and $\mathbf{Y}_{\rm sc}$. The MoC-based model (ULM) used 12 pole-residue terms for the fitting of $\mathbf{Y}_c$ and 14 terms for the fitting of $\mathbf{H}$ (single delay group). Taking into account both line ends, this gives a total of 52 terms for ULM compared to 36 terms for FLE (all terms with residue matrix of size 3×3). Clearly, the FLE is here computationally more efficient than ULM.

IX. CONCLUSION

This paper has introduced a new transmission-line model for the simulation of electromagnetic transients, the FLE. The FLE is obtained by decomposing the nodal admittance matrix $\mathbf{Y}_{\rm nod}$ into blocks that represent open-circuit and $(\mathbf{Y}_{\rm oc})$ short-circuit $(\mathbf{Y}_{\rm sc})$ conditions of the half-length line. These blocks are subjected to rational fitting with relative error control by inverse magnitude weighting and passivity enforcement. The resulting model is included in the EMT program environment via a

Norton equivalent. The following conclusions can be made about the FLE approach.

1) The modeling is performed in the phase domain without assumptions of a constant transformation matrix. The approach is therefore applicable to untransposed overhead lines and underground cables.
2) The FLE is capable of retaining the relative accuracy of the eigenvalues of $\mathbf{Y}_{\mathrm{nod}}$, even with a large eigenvalue ratio. This is contrary to a direct fitting of $\mathbf{Y}_{\mathrm{nod}}$ where the small eigenvalues (low frequencies) are often corrupted. In addition, the fitting and passivity enforcement steps are faster and more reliable than with a direct fitting of $\mathbf{Y}_{\mathrm{nod}}$.
3) The accurate representation of all eigenvalues of $\mathbf{Y}_{\mathrm{nod}}$ allows the model to be used with arbitrary terminal conditions, without danger of large error magnifications.
4) Although the FLE is highly accurate, it is computationally inferior to MoC-based phase-domain models when wide frequency bands need to be modeled.
5) By limiting the application of FLE to situations where the simulation time step is bigger than the line travel time, the FLE becomes comparable or even faster than the MoC counterpart. This comes in addition to the fact that the MoC approach is not even applicable with this type of time step. Compared to the usage of PI-sections, the FLE is more accurate since it takes into account the frequency-dependent effects of the line.

REFERENCES

[1] A. Semlyen and A. Dabuleanu, "Fast and accurate switching transient calculations on transmission lines with ground return using recursive convolutions," *IEEE Trans. Power App. Syst.*, vol. PAS-94, no. 2, pt. 1, pp. 561–575, Mar./Apr. 1975.

[2] J. R. Marti, "Accurate modelling of frequency-dependent transmission lines in electromagnetic transient simulations," *IEEE Trans. Power App. Syst.*, vol. PAS-101, no. 1, pp. 147–157, Jan. 1982.

[3] T. Noda, N. Nagaoka, and A. Ametani, "Phase domain modeling of frequency-dependent transmission lines by means of an ARMA model," *IEEE Trans. Power Del.*, vol. 11, no. 1, pp. 401–411, Jan. 1996.

[4] A. Morched, B. Gustavsen, and M. Tartibi, "A universal model for accurate calculation of electromagnetic transients on overhead lines and underground cables," *IEEE Trans. Power Del.*, vol. 14, no. 3, pp. 1032–1038, Jul. 1999.

[5] EMTP Theory Book. Portland, OR, Aug. 1986, prepared by H.W. Dommel. Bonneville Power Administration, Oregon.

[6] A. I. Ibrahim, S. Henschel, A. C. Lima, and H. W. Dommel, "Applications of a new EMTP line model for short overhead lines and cables," *Elect. Power Energy Syst.*, vol. 24, no. 8, pp. 639–645, 2002.

[7] B. Gustavsen and C. Heitz, "Modal vector fitting: A tool for generating rational models of high accuracy with arbitrary terminal conditions," *IEEE Trans. Adv. Packag.*, to be published.

[8] B. Gustavsen and A. Semlyen, "Rational approximation of frequency domain responses by vector fitting," *IEEE Trans. Power Del.*, vol. 14, no. 3, pp. 1052–1061, Jul. 1999.

[9] B. Gustavsen, "Improving the pole relocating properties of vector fitting," *IEEE Trans. Power DeL.*, vol. 21, no. 3, pp. 1587–1592, Jul. 2006.

[10] S. Boyd and L. O. Chua, "On the passivity criterion for LTI n-ports," *Circuit Theory Appl.*, vol. 10, pp. 323–333, 1982.

[11] A. Semlyen and B. Gustavsen, "A half-size singularity test matrix for fast and reliable passivity assessment of rational models," *IEEE Trans. Power Del.*, vol. 24, pp. 345–351, 1, Jan. 2009.

[12] D. Saraswat, R. Achar, and M. S. Nakhla, "A fast algorithm and practical considerations for passive macromodeling of measured/simulated data," *IEEE Trans. Adv. Packag.*, vol. 27, no. 1, pp. 57–70, Feb. 2004.

[13] S. Grivet-Talocia, "Passivity enforcement via perturbation of hamiltonian matrices," *IEEE Trans. Circuits Syst. I, Reg. Papers*, vol. 51, no. 9, pp. 1755–1769, Sep. 2004.

[14] B. Gustavsen, "Fast passivity enforcement for pole-residue models by perturbation of residue matrix eigenvalues," *IEEE Trans. Power Del.*, vol. 23, no. 4, pp. 2278–2285, Oct. 2008.

[15] B. Gustavsen and A. Semlyen, "Enforcing passivity for admittance matrices approximated by rational functions," *IEEE Trans. Power Syst.*, vol. 16, no. 1, pp. 97–104, Feb. 2001.

[16] B. Gustavsen and O. Mo, "Interfacing convolution based linear models to an electromagnetic transients program," in *Proc. Int. Conf. Power Systems Transients*, Lyon, France, Jun. 4–7, 2007, p. 6.

[17] C. Chen, E. Gad, M. Nakhla, and R. Achar, "Passivity verification in delay-based macromodels of multiconductor electrical interconnects," *IEEE Trans. Adv. Packag.*, vol. 30, no. 2, pp. 246–256, May 2007.

[18] "Fast delay-less interconnect macromodeling and simulation by assumption of a constant eigenvector matrix," in *Proc. 12th IEEE Workshop Signal Propagation on Interconnects*, Avignon, France, May 12–15, 2008, pp. 1–4.

Bjørn Gustavsen (M'94–SM'03) was born in Norway in 1965. He received the M.Sc. and Dr.Ing. degrees from the Norwegian Institute of Technology (NTH), Trondheim, in 1989 and 1993, respectively.

Since 1994, he has been with SINTEF Energy Research, Trondheim. His interests include simulation of electromagnetic transients and modeling of frequency-dependent effects. In 1996, he was a Visiting Researcher at the University of Toronto, Toronto, ON, Canada, and in 1998, he was with the Manitoba HVDC Research Centre, Winnipeg, MB, Canada.

Dr. Gustavsen. was a Marie Curie Fellow at the University of Stuttgart, Germany, from 2001 to 2002.

Adam Semlyen (LF'97) was born in 1923 in Romania. He received the Dipl. Ing. and Ph.D. degrees.

He began his career in Romania with an electric power utility and held academic positions at the Polytechnic Institute of Timisoara. In 1969, he joined the University of Toronto, Toronto, ON, Canada, where he is a Professor in the Department of Electrical and Computer Engineering, emeritus since 1988. His research interests include steady state and dynamic analysis as well as computation of electromagnetic transients in power systems.